ARTICLE

Photofragment Imaging of HNCO Decomposition at 210 nm: the Primary NH($a^1\Delta$)+CO($X^1\Sigma^+$) Channel†

Hua Wang[a], Shi-lin Liu[a*], Jie Liu[b], Feng-yan Wang[b], Bo Jiang[b], Xue-ming Yang[b*]

a. Hefei National Laboratory for Physical Sciences at Microscale, Department of Chemical Physics, University of Science and Technology of China, Hefei 230026, China;
b. State Key Laboratory of Molecular Reaction Dynamics, Dalian Institute of Chemical Physics, Chinese Academy of Science, Dalian 116023, China

(Dated: Received on June 3, 2007; Accepted on June 19, 2007)

The photodissociation of isocyanic acid (HNCO) on the first excited singlet state following the excitation at 210 nm was investigated with an ion velocity slice imaging technique by probing the CO fragment. It was found from the (2+1) resonance-enhanced multi-photon ionization (REMPI) spectrum that the CO fragments are rotationally hot with population up to J_{max}=50. The velocity imagings of the CO fragments at J_{CO}=30 and 35 indicate that formation of NH($a^1\Delta$)+CO($X^1\Sigma^+$, v=0) is the predominant dissociation channel at 210 nm. From analysis of the CO fragment translational energy distributions, the NH($a^1\Delta$) fragment was observed to be rotationally cold, about half of the available energy was partitioned into the translational motion of fragments after dissociation, and the NH($a^1\Delta$)+CO($X^1\Sigma^+$) dissociation threshold was determined at 42738±30 cm^{-1}. From analysis of the CO fragment angular distributions, the dissociation anisotropy parameter β was found to be negative, and increasing with the rotational quantum number of the NH fragment, i.e., from −0.75 at J_{NH}=2-4 to −0.17 at J_{NH}=11. Impulsive direct and vertical dissociation process of HNCO on the singlet state at 210 nm was confirmed experimentally. A classical impact dissociation model was employed to explain the dependence of the β value on the rotational excitation of the NH fragment.

Key words: Isocyanic acid, Dissociation dynamics, Velocity slice imaging, Dissociation energy, Fragment angular distribution, Translational energy distribution

I. INTRODUCTION

Isocyanic acid (HNCO) is a 16-valence-electron molecule with C_s symmetry, and plays a significant role in the rapid reduction of nitrogen oxides in the atmosphere [1,2]. It is also a model molecule to study the photodissociation dynamics at a state-to-state level, since the fragment pair can be ro-vibrationally probed. The absorption spectrum of HNCO in the UV range of 180-280 nm is broad and continuous with weakly superimposed vibrational structures above 220 nm [3]. This spectrum has been assigned to the electronic transition from the ground state S_0 to the lowest excited singlet state S_1. The N−C−O angle at the S_1 state is about 120°, which is quite different from linear structure of N−C−O at the ground S_0 state [3,4].

The photodissociation dynamics of HNCO on the S_1 state is complicated by the participation of three potential energy surfaces (PESs), S_0, S_1, and the triplet T_1 states [5-20]. There are three energetically possible dissociation channels from the S_1 state to generate three sets of products, ^{3}NH+CO, H+NCO, and ^{1}NH+CO [17],

$$\mathrm{HNCO(S_1)} \longrightarrow \mathrm{NH}(X^3\Sigma^-) + \mathrm{CO}(X^1\Sigma^+) \quad (1)$$
$$D_0 = 30060\ \mathrm{cm^{-1}}$$
$$\longrightarrow \mathrm{H}(^2\mathrm{S}) + \mathrm{NCO}(X^2\Pi) \quad (2)$$
$$D_0 = 38370\ \mathrm{cm^{-1}}$$
$$\longrightarrow \mathrm{NH}(a^1\Delta) + \mathrm{CO}(X^1\Sigma^+) \quad (3)$$
$$D_0 = 42750\ \mathrm{cm^{-1}}$$

Channel (1) is a spin-forbidden dissociation pathway, and requires intersystem crossing by which HNCO eventually reaches the triplet state T_1 and then dissociates. Theoretical studies showed that the dissociation of this channel follows the process $S_1 \rightarrow S_0 \rightarrow T_1 \rightarrow$products [18]. Both Channels (2) and (3) are spin-allowed adiabatic dissociation pathways [8-17]. Channel (2) breaks the N−H bond to form H(^{2}S)+NCO($X^2\Pi$). Since this channel has an exit barrier of about 8100 cm^{-1} along the N−H stretching coordinate [9,15,16], dissociation of Channel (2) is likely to proceed by internal conversion to S_0 followed by adiabatic dissociation [13,18]. Due to interactions between the three electronic states, i.e., the internal conversion between S_1 and S_0 states, and the intersystem crossings between S_1 and T_1 states and between S_0 and T_1 states, the branching ratio of the three dissociation channels varies with the photolysis wavelength. Berghout *et al.* measured the relative yields of ^{3}NH, NCO and ^{1}NH fragments at dissociation wavelengths ranging from 260 nm to 220 nm with laser-

†Part of the special issue "Cun-hao Zhang Festschrift".
*Authors to whom correspondence should be addressed. E-mail: slliu@ustc.edu.cn, Tel: +86-551-3602323, Fax: +86-551-3602323, E-mail: xmyang@dicp.ac.cn, Tel: +86-411-84695174

induced fluorescence (LIF) spectroscopy [19]. Their results showed a picture in which each higher energy channel dominates the product yield as it becomes energetically accessible, i.e., with the production of about 70% H+NCO (Channel (2)) and 30% ^{3}NH+CO (Channel (1)) at energies as high as 200 cm^{-1} above the threshold for formation of NCO, and the production of about 80% ^{1}NH+CO (Channel (3)) and 15% H+NCO (Channel (2)) at energies as high as 3000 cm^{-1} above the threshold for formation of ^{1}NH. It had been proposed by many works [10-13,17] that direct dissociation would occur on the S_1 state to form ^{1}NH+CO (Channel (3)) when the photolysis energy exceeds the corresponding dissociation threshold, but this remained unconfirmed experimentally.

There are several works focusing on the determination of dissociation threshold of Channel (3). Spiglanin *et al.* measured the dissociation energy $D_0(^1\text{NH+CO})$ to be 41530±150 cm^{-1} by determining the energy contents of the ^{1}NH fragment with saturated LIF and the CO co-fragment with (2+1) REMPI at wavelengths near the threshold [5-7]. Reisler *et al.* measured the dissociation energy with ion imaging method by detecting the CO fragment [13,17]. They gave a value of 42765±25 cm^{-1} in Ref.[13], and re-measured the dissociation energy in Ref.[17] to be 42750±25 cm^{-1} with an improved ion imaging technique, called ion velocity mapping. As can be seen, the values for dissociation energy of Channel (3) reported by different groups are inconsistent.

The photodissociation dynamics of HNCO at energies well above the threshold of Channel (3) had scarcely been investigated. Only Kawasaki *et al.* studied the dissociation dynamics at λ=217 nm, but with an old fashioned ion imaging method [11]. The dissociation dynamics at excitation wavelengths λ<230 nm are presently the least understood compared to Channels (1) and (2).

In this work, the authors used the newly developed technique, ion velocity slice imaging, to study the dissociation dynamics of HNCO at λ=210 nm (about 5000 cm^{-1} above the dissociation threshold). The reason to choose the studied wavelength at 210 nm is the convenience of generation by dye laser and its high excitation photon energy. The internal state populations of ^{1}NH and CO fragments and the fragmentation angular distributions are obtained from the CO velocity imaging, and more precise dissociation threshold $D_0(^1\text{NH})$ is expected to be obtained due to the higher resolution of the ion velocity slice imaging used in this work.

II. EXPERIMENTS

The experimental set-up had been described in detail previously [21-23]. To improve the resolution of ion velocity slice imaging, the ion optics of a TOF mass spectrometer were modified, with a design similar to that reported by Lin *et al.* [24]. A total of 31 circular stainless plates were used to build two parts of a homogeneous electrostatic field, with their voltages controlled by precision resistors. Six plates constitute a weak field (∼24.7 V/cm for total voltage 900 V) to extract the ions, four plates constitute a transition region, and the last 21 plates form a strong field (∼54 V/cm) to accelerate the ions. In this case, an ion-focusing system was built essentially by the transition from low field region to the high field, and the focusing condition can be achieved by simply varying the ratio of field strengths between the two regions. During the experiment, a pulsed high voltage (Directed Energy Inc., PVM-4210) with 50 ns duration was applied to the microchannel plates (MCP) to gate the CO^+ ion packet. Calibrations of the translation energy had been done by measuring the velocity imaging of the O^+ fragments from the multi-photon dissociation/ionization of O_2 at 224.999 nm [25].

A sample of ∼2% HNCO/He mixture at the stagnation pressure of 1.2 atmosphere was expanded supersonically into a vacuum chamber through a pulsed valve (General Valve, Series 9). The jet-cooled molecular beam was collimated by a skimmer, and was then intercepted by two linearly polarized laser beams: a dissociation laser and a probe laser. The two laser beams counter-propagated with each other, and were focused by two quartz lenses into the chamber. The two laser beams were generated by the doubled outputs of two nano-second dye lasers (Lambda Physiks LPD3000 and FL2002) pumped simultaneously by a XeCl excimer laser (Lambda Physiks LPX200). The HNCO molecules in the jet were photolyzed by the dissociation laser to produce CO fragments, and the CO fragments were ionized by the probe laser via the $B^1\Sigma^+ \leftarrow\leftarrow X^1\Sigma^+$ (2+1) REMPI process. The produced CO^+ fragment ions were accelerated by the velocity focusing electric fields, and projected onto a dual MCP backed by a phosphor screen. The transient images on the phosphor screen were captured by a thermoelectrically cooled charge-coupled-device (CCD) camera and accumulated on the CCD chip. Simultaneously, the total emission from the phosphor screen was recorded by a photo-multiplying tube (PMT), and displayed on an oscilloscope in order to optimize the experiment and monitor the ion signal during the image data acquisition process. The ion signal from the PMT was averaged by a Boxcar integrator and sent to a PC to obtain the REMPI spectrum of the CO fragment. To measure the velocity image of the CO fragment at a certain rotational level, the wavelength of the probe laser was scanned around the corresponding rotational line to cover the entire Doppler width. Since the CO^+ spatial distribution was cylindrically symmetric around the electric vector of the dissociation laser, the image slicing through the ion packet center constructed the actual 3-dimensional (3D) velocity distribution of the CO fragment.

HNCO was prepared by heating KOCN and stearic acid at about 80 °C [26], purified by distilling from −77 °C to −196 °C, and stored in a liquid-N_2 vessel.

DOI:10.1088/1674-0068/20/04/388-394

During the experiments, pure He gas with a pressure of 121 kPa passed through the liquid HNCO at −40 °C to carry out the HNCO molecules, and the gas mixture was let into the vacuum chamber.

III. RESULTS

A. (2+1) REMPI spectrum of CO fragment

Figure 1 shows the (2+1) REMPI spectra of CO fragments in the region of Q-branch of the $B^1\Sigma^+$ (v=0)←←$X^1\Sigma^+$ (v=0) transition. Spectra related with other vibrational states of CO($X^1\Sigma^+$, $v\neq0$) were not observed. Two spectra are included in the figure: one was obtained with the combination of dissociation laser at λ=210 nm and the probe laser (solid line), and the other was obtained with the probe laser only (dashed line). As can be seen clearly, the CO fragment generated by the probe laser was rotationally cold, while that generated by dissociation laser was rotationally hot. The CO fragments populated at J_{CO}>20 are definitely generated from the photolysis of HNCO by the 210 nm dissociation laser. As the figure shows, rotational populations of CO fragments up to J_{CO}=50 were observed. This indicates that the bending (ν_2) mode vibration of HNCO was highly excited by the 210 nm dissociation laser from the linear ground state, causing a twist torsion along the dissociation coordinate. In order to avoid interference from the probe laser and to study the dissociation dynamics at 210 nm, the wavelengths of probe laser were fixed separately at positions of the J_{CO}=35 and 30 rotational levels to measure the CO fragment ion velocity images.

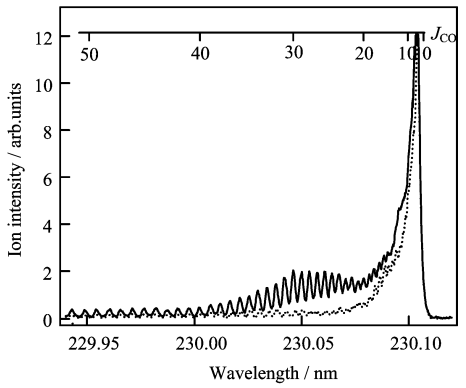

FIG. 1 The (2+1) REMPI spectra of CO in the region of Q-branch via $B^1\Sigma^+$←←$X^1\Sigma^+$ electronic transition at around 230 nm. The spectra were obtained with the combination of dissociation laser at λ=210 nm and the probe laser (solid line), and the probe laser only (dashed line), respectively. As can be seen, the CO fragment generated by the probe laser was rotationally cold, while that generated by the dissociation laser was rotationally hot.

B. Total released kinetic energy distributions

Shown in Fig.2 (a) and (b) are the slicing images by probing the CO fragments at J_{CO}=35 and 30 rotational levels. These images were accumulated for 35000 laser shots, and the gate duration was 60 ns for slicing the ion packet in the time scale. The arrow shows the direction of the electric vector of the photolysis laser. The light points at the image center originate from the CO^+ ion signals by the probe laser. Fortunately, they contribute very little to the total released kinetic energy distribution.

By integrating the signal intensities in Fig.2(a) and (b) over the entire angle, the velocity distribution $P(v)$ of CO fragment and then the total released kinetic energy distribution $P(E)$ were obtained, as shown in Fig.2(c) and (d). As can be seen, the NH fragment is rotationally cold, in contrast to its partner fragment CO which is the rotationally hot. Since the energy gap between the low rotational levels is so small, the NH rotational levels could not be resolved completely at J_{NH}<6 levels. The rotational excitation of NH is up to J_{NH}=11-13, tending to the higher rotational levels with the increasing of CO rotational levels. This is consistent with the measurements by Sanov *et al.* [13], and can be understood by the conservation of angular momentum before and after dissociation. Panels (e) and (f) show the relation of $\ln[P_{J_{NH}}/(2J+1)]$ with $J(J+1)$, where $P_{J_{NH}}$ denotes the rotational population of NH at J_{NH} level which was derived from the de-convolution of measured $P(E)$ with Gaussian profiles. The nonlinear relationship between $\ln[P_{J_{NH}}/(2J+1)]$ and $J(J+1)$ indicates a non-Boltzman population distribution of NH fragment, meaning that a direct dissociation of HNCO occurs at 210 nm.

The dissociation threshold energy $D_0(^1\text{NH})$ of Channel (3), ^{1}NH+CO, can be derived from the measured $P(E)$ following energy conservation,

$$h\nu - D_0(^1\text{NH}) = E_{\text{int}}(\text{CO}) + E_{\text{int}}(\text{NH}) + E_{\text{trans}} \quad (4)$$

where $h\nu$ denotes the dissociation photon energy, $h\nu - D_0(^1\text{NH})$ is the total available energy, E_{int}(CO) and E_{int}(NH) represent the internal energy of CO and NH fragments, respectively, including electronic, vibrational and rotational energies. E_{trans} represents total translational energy released after dissociation. From each ion image of CO at certain J_{CO}, and from the released kinetic energy of NH at certain J_{NH} in its corresponding $P(E)$ spectrum, the $D_0(^1\text{NH})$ value can be easily obtained. Figure 3 shows the estimated values of $D_0(^1\text{NH})$ by using 13 rotational levels of NH and two rotational levels of CO. The averaged value of $D_0(^1\text{NH})$ was finally determined as $D_0(^1\text{NH})$=42738±30 cm^{-1}. Therefore, the total available energy in this experiment was about 4880 cm^{-1}.

The most probable translational energy $\langle E_{\text{trans}}\rangle$ can be derived from the measured $P(E)$ in Fig.2(c) and (d)

DOI:10.1088/1674-0068/20/04/388-394

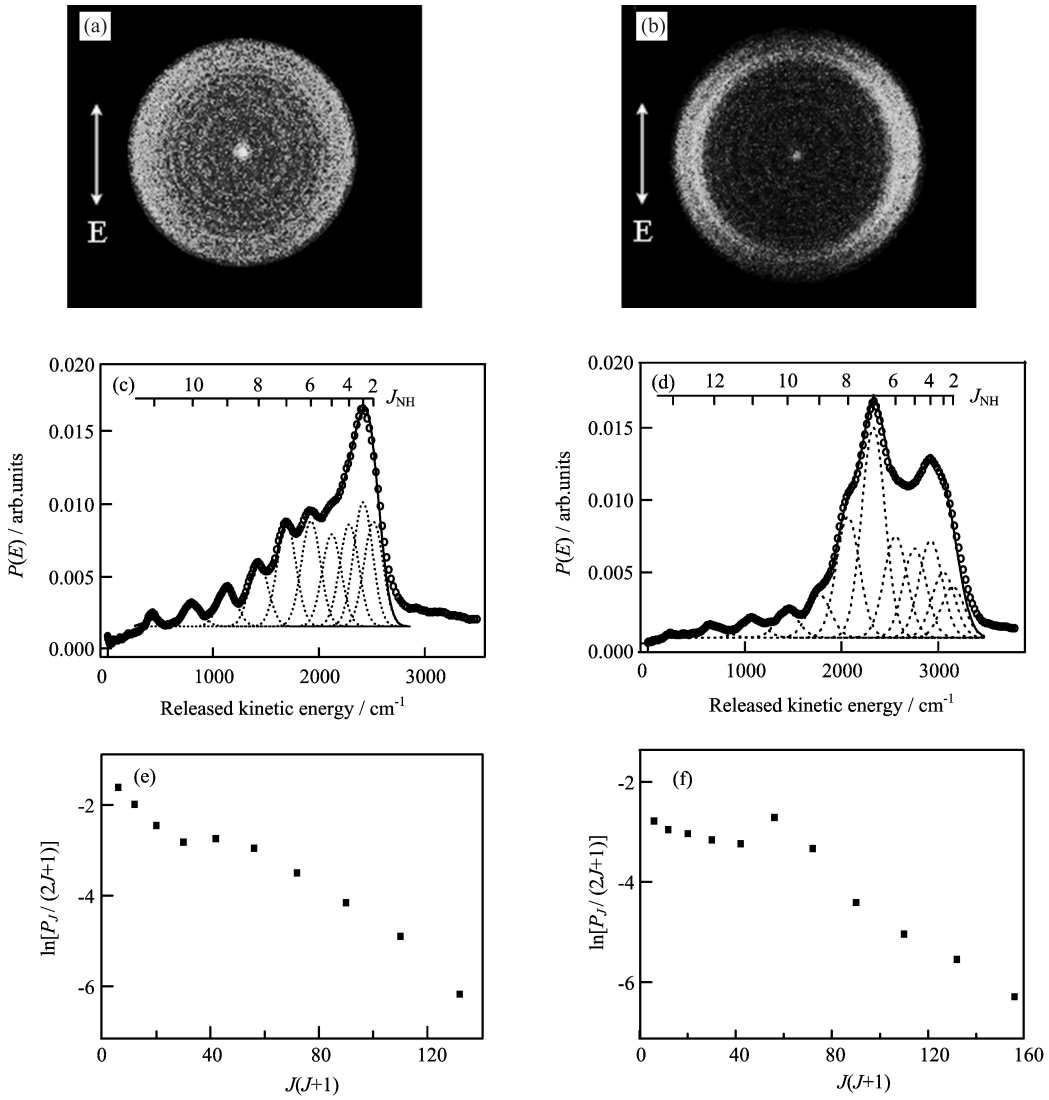

FIG. 2 Slicing images of CO($X^1\Sigma^+$, v=0) fragment at dissociation wavelength of 210 nm and probing at J_{CO}=35 (a) and J_{CO}=30 (b) rotational levels. The arrows indicate the direction of the electric vector of the photolysis laser. (c) and (d) show the total released kinetic energy distributions obtained from images (a) and (b), respectively, and are assigned to J_{NH} rotational levels. Dashed lines represent the de-convolution into the contributions from individual J_{NH} levels, by fitting $P(E)$ with Gaussian profiles. (e) and (f) show the plots of $\ln[P_J/(2J+1)]$ *vs.* $J(J+1)$, where P_J denotes the rotational population of NH obtained from (c) and (d), respectively.

from the formula,

$$\langle E_{\rm trans}\rangle = \frac{\int P(E)E{\rm d}E}{\int P(E){\rm d}E} \tag{5}$$

From the CO image at J_{CO}=35, $\langle E_{\rm trans}\rangle$ was determined to be 1997 cm^{-1}, about 41% of the total available energy, and from the CO image at J_{CO}=30, $\langle E_{\rm trans}\rangle$ was 2438 cm^{-1}, about 50% of the available energy. The partitioning of available energy into fragment translational motion is close to the previous conclusion (∼40%) for photodissociating HNCO at 217 nm [11], but a little bit larger than the previous result.

C. Photofragment angular distribution

The fragmentation angular distributions $P(\theta,v)$ for a certain speed v of the CO fragment can be obtained by collecting the ion signal intensities from the points with speed v at each angle θ in the recorded images in Fig.2(a) and (b), where θ is the angle between the laser polarization direction and the recoil velocity of the CO fragment. The relation of $P(\theta,v)$ with θ obeys the standard recoil anisotropy function [27],

$$P(\theta, v) \propto 1 + \beta P_2(\cos(\theta)) \tag{6}$$

where β is the photofragment recoil anisotropy parameter and P_2 is the second-order Legendre polyno-

DOI:10.1088/1674-0068/20/04/388-394

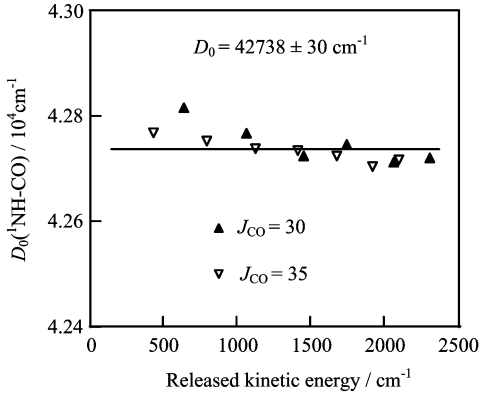

FIG. 3 The threshold dissociation energy to form NH($a^1\Delta$)+CO($X^1\Sigma^+$), obtained from slicing images of CO at J_{CO}=30 and J_{CO}=35 levels, and from their corresponding kinetic energies of NH at different J_{NH} levels.

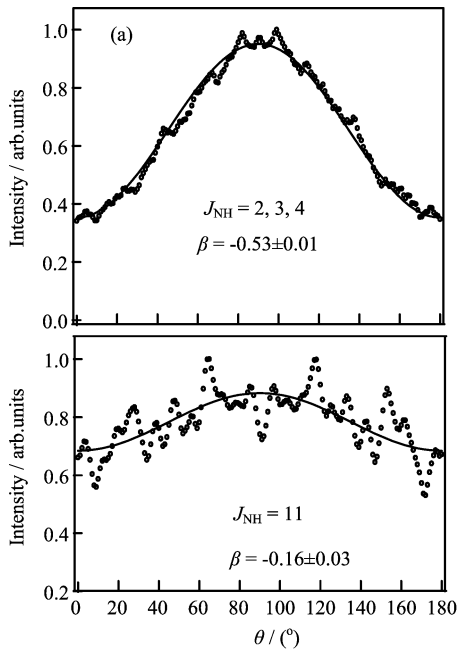

FIG. 4 The product angular distributions (circle) of CO(v=0, J_{CO}=35) for J_{NH}=2-4 and J_{NH}=11 rotational levels of NH when photodissociating HNCO at 210 nm, along with their least-squares fittings to Eq.(6).

mial. Figure 4 and 5 show the photofragment angular distributions at low and high rotational levels of NH (J_{NH}=2-4 and J_{NH}=11) from images of CO at J_{CO}=35 and J_{CO}=30, and their corresponding simulations with Eq.(6). The minimum value, −0.75, was obtained at J_{NH}=2-4 and J_{CO}=30, indicating a direct and vertical dissociation of HNCO on S1 state at 210 nm, which is consistent with non-Boltzman population distribution of NH fragments. It is worthy of note that in both the cases of J_{CO}=30 and 35, the anisotropy parameter increases with the rotational excitation of NH and tends

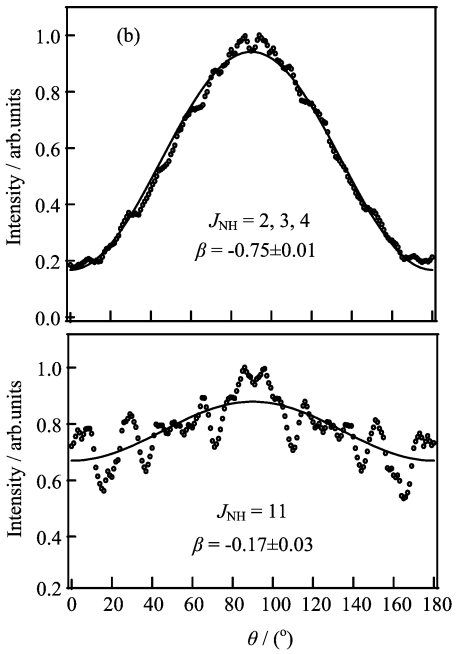

FIG. 5 The product angular distributions (circle) of CO(v=0, J_{CO}=30) for J_{NH}=2-4 and J_{NH}=11 rotational levels of NH when photodissociating HNCO at 210 nm, along with their least-square fittings to Eq.(6).

to zero.

IV. DISCUSSION

A. Rotational population of CO fragment

The relative rotational population cannot be obtained directly from Fig.1, since it is a linear spectrum and the two-photon excitation cross-section is rotationally dependent. Ignoring the effect of predissociation on the CO $B^1\Sigma^+$ state, the REMPI signal intensity (I) is proportional to the rotational population $N_{J''}$ and the two-photon transition cross-section $\sigma_{J'\leftarrow J''}$,

$$I \propto N_{J''}\sigma_{J'\leftarrow J''} \tag{7}$$

Since $\sigma_{J'\leftarrow J''}$ is J''-dependent, it is necessary to get the expression of $\sigma_{J'\leftarrow J''}$ to estimate the rotational distribution $N_{J''}$ from the REMPI spectrum. Theoretical study [28] has showed that for linearly polarized light the Q-branch transition cross-section of the $\Sigma\leftarrow\leftarrow\Sigma$ transition can be expressed by Eq.(8) (for simplicity, we use J to stand for J''),

$$\sigma_{||} = \frac{(2J+1)}{9}{\mu_I}^2 + \frac{(2J+1)J(J+1)}{45(2J-1)(2J+3)}{\mu_S}^2 \tag{8}$$

where μ_I and μ_S represent the transition dipole factors for linearly and circularly polarized light, respectively. Moreover, the ratio of cross-sections between linearly and circularly polarized light, $\sigma_{||}/\sigma_{cc}$, can be expressed

DOI:10.1088/1674-0068/20/04/388-394

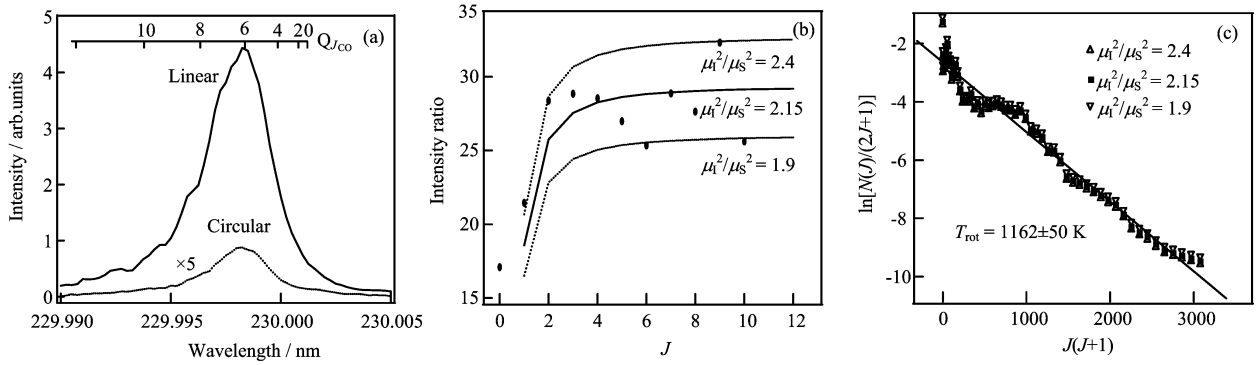

FIG. 6 (a) The (2+1) REMPI spectra of jet-cooled CO recorded with linearly (solid line) and circularly polarized lasers at 230 nm. (b) The rotational dependence of the spectral intensity ratio between those obtained with linearly and circularly polarized lasers (dot), and their simulations with Eq.(9) to determine the factor $\mu_I{}^2/\mu_S{}^2$ (see the text). (c) The relation of determined relative rotational population of CO fragment from Fig.1 with J, giving a rotational temperature of 1162 K.

as,

$$\frac{\sigma_{||}}{\sigma_{cc}} = \frac{10(2J+3)(2J-1)}{3J(J+1)}\frac{\mu_{\rm I}{}^2}{\mu_{\rm S}{}^2} + \frac{2}{3} \qquad (9)$$

The factor $\mu_{\rm I}{}^2/\mu_{\rm S}{}^2$ was measured by recording the (2+1) REMPI spectra of supersonically cooled CO with linearly and circularly polarized lasers at around 230 nm. From the spectral intensity ratio at certain J, $\mu_I{}^2/\mu_S{}^2$ should be determined. The REMPI spectra of CO at ~230 nm were obtained with two polarization lasers, as shown in Fig.6(a). The ratio $\mu_{\rm I}{}^2/\mu_{\rm S}{}^2$ was estimated to be 2.15±0.2, as shown in Fig.6(b) by fitting the spectral intensity ratio to Eq.(9). In this way, the dependence of two-photon excitation cross-section of CO upon the rotational level J could be obtained from Eq.(8), and the relative rotational populations $N(J)$ of CO fragment could be in turn determined from the REMPI spectrum in Fig.1. Figure 6(c) displays three plots of $\ln[N(J)/(2J+1)]$ *vs.* $J(J+1)$, which were obtained with $\mu_{\rm I}{}^2/\mu_{\rm S}{}^2$=2.4, 2.15, and 1.9. These three plots are almost the same, meaning that the determined CO relative populations are reliable. A linear fitting to these plots yields a rotational temperature of 1162±50 K. The high temperature implies that the CO fragment from the photodissociation of HNCO at 210 nm is highly rotationally excited, which again confirms the direct dissociation dynamics in the S_1 state of HNCO to generate NH($a^1\Delta$)+CO($X^1\Sigma^+$) products.

B. Dissociation energy $D_0(^1\mathrm{NH})$

As mentioned in the Introduction, the dissociation threshold of the first direct dissociation pathway, Channel (3), remains uncertain. In this work, HNCO was photo-dissociated at 210 nm, and the kinetic energy distributions of the CO fragment was probed at two rotational levels using a newly developed technique, i.e., ion velocity slicing image. The $D_0(^1\mathrm{NH})$ value was measured at 42738±30 cm^{-1} by simulating higher rotational levels of NH from the $J_{\rm NH}$=6 to 13 levels. In principle, this value should be more accurate than previous results.

C. Recoil anisotropy parameter

The photofragment recoil anisotropy parameter β when dissociating HNCO at 217 nm has been measured by Kawasaki *et al.* to be β=−0.7±0.2 [11], indicating that the recoil velocity of the CO fragment is almost perpendicular to the vector of transition dipole moment. However, Sanov *et al.* did not observe such a negative value of β in their experiment [13]. They declared that it was caused by their incomplete integration over the full extent of the Doppler profile when recording the CO velocity imaging. In this work, the recoil anisotropy parameters were obtained with a minimum value β=−0.75±0.01, which is in agreement with Kawasaki *et al.*'s results [11]. But the variation of β value with the rotational excitation of NH had not been observed in both Refs.[11] and [13].

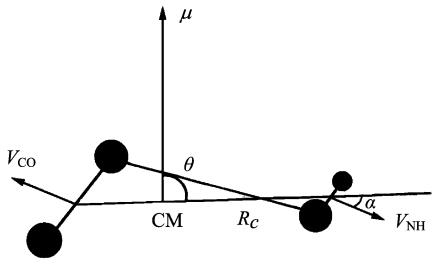

FIG. 7 Critical geometry and orientation of HNCO. R_c is the distance between the centers of mass (CM) of CO and NH moieties, μ is the transition dipole moment vector, V is the fragment recoil velocity. θ is the angle between μ and the direction of R_c, and α is the angle between V and R_c. Angle α which is correlated with rotational excitation of NH moiety, determines the deviation from axial recoil.

From the images obtained at $J_{\rm CO}$=35 and 30, we notice that the recoil anisotropy parameter β increases

DOI:10.1088/1674-0068/20/04/388-394

distinctly with the NH rotational excitation and tends to zero. This phenomenon had been also found in the photodissociation studies of N_2O [29] and NO_2 [30]. An impact model was employed to illuminate this phenomenon. Figure 7 shows the sketch map of this model in the HNCO molecule, where R_c is the distance between the centers of mass (CM) of CO and NH moieties, θ is the angle between the polarization vector of photolysis laser and R_c, and α is the angle between the recoil velocity vector (V) and R_c. In this case, β can be expressed as [30],

$$\beta = 2P_2[\cos(\theta + \alpha)] \tag{10}$$

Since the angle α is a function of the rotational level J of fragments, the β value should vary with the rotational excitation of dissociation products. The rotational constant of NH is 10 times bigger than that of CO, so the β value should be more sensitive to the rotational excitation of NH, while the CO moiety could be simply regarded as one heavy atom. When HNCO molecule is excited to the S_1 state, the transition dipole moment is vertical to the molecular plane and HNCO in the S_1 state is kept in a planar geometry. Moreover, the planar structure almost does not change, so that the angle θ is always close to 90° at the time of direct dissociation. Therefore, the β value is close to -1 when the angle α is small corresponding to a low NH rotational excitation, and tends to zero with the increase of angle α corresponding to the high NH rotational excitation. The qualitative illumination of the variation of β value in the HNCO dissociation is consistent with the experimental observations here. The same model can also be applied to explain the similar phenomena of CO rotational state in principle while taking the NH moiety as an atom.

V. CONCLUSION

Photodissociation of HNCO at 210 nm, whose excitation energy is well above the dissociation threshold to form NH($a^1\Delta$)+CO($X^1\Sigma^+$) products, was investigated using an ion velocity slice imaging technique. The rotational distribution of the CO photofragment was obtained from the (2+1) REMPI spectrum at around 230 nm. The total released kinetic energy distribution and fragments angular distribution of CO fragment at rotational levels J_{CO}=30 and 35 were studied. The dissociation threshold energy was estimated as $D_0(^1\text{NH-CO})$=42738±30 cm^{-1}, and the recoil anisotropy parameter β was found to have a minimum value β=−0.75±0.01 at the low NH rotational excitations and to increase with J_{NH}. This experiment give the first confirmation of rapid direct impulsive dissociation of HNCO in the S_1 state at 210 nm to form NH($a^1\Delta$)+CO($X^1\Sigma^+$). An impact dissociation model was used to explain the variation of β value with the NH rotational excitation.

VI. ACKNOWLEDGMENTS

This work was supported by the National Natural Science Foundation of China (No.20533070, No.20573100).

[1] R. A. Perry and D. L. Siebers, Nature **324**, 657 (1986).
[2] J. A. Miller and C. T. Bowman, Int. J. Chem. Kinet. **23**, 289 (1991).
[3] R. N. Dixon and G. H. Kirby, Trans. Faraday Soc. **64**, 2002 (1968).
[4] D. R. Yarkony, J. Chem. Phys. **114**, 2614 (2001).
[5] T. A. Spiglanin, R. A. Perry, and D. W. Chandler, J. Phys. Chem. **90**, 6184 (1986).
[6] T. A. Spiglanin, R. A. Perry, and D. W. Chandler, J. Chem. Phys. **87**, 1568 (1987).
[7] T. A. Spiglanin and D. W. Chandler, J. Chem. Phys. **87**, 1577 (1987).
[8] J. Zhang, M. Dulligan, and C. Wittig, J. Phys. Chem. **99**, 7446 (1995).
[9] S. S. Brown, C. M. Cheatum, D. A. Fitzwater, and F. F. Crim, J. Chem. Phys. **105**, 10911 (1996).
[10] S. S. Brown, H. L. Berghout, and F. F. Crim, J. Chem. Phys. **105**, 8103 (1996).
[11] M. Kawasaki, Y. Sato, K. Suto, Y. Matsumi, and S. H. S. Wilson, Chem. Phys. Lett. **251**, 67 (1996).
[12] M. Zyrianov, T. Droz-Georget, A. Sanov, and H. Reisler, J. Chem. Phys. **105**, 8111 (1996).
[13] A. Sanov, T. Droz-Georget, M. Zyrianov, and H. Reisler, J. Chem. Phys. **106**, 7013 (1997).
[14] T. Droz-Georget, M. Zyrianov, H. Reisler, and D. W. Chandler, Chem. Phys. Lett. **276**, 316 (1997).
[15] J. J. Klossika, H. Floethmann, C. Beck, R. Schinke, and K. Yamashita, Chem. Phys. Lett. **276**, 325 (1997).
[16] J. E. Stevens, Q. Cui, and K. Morokuma, J. Chem. Phys. **108**, 1452 (1998).
[17] M. Zyrianov, T. Droz-Georget, and H. Reisler, J. Chem. Phys. **110**, 2059 (1999).
[18] A. L. Kaledin, Q. Cui, M. C. Heaven, and K. Morokuma, J. Chem. Phys. **111**, 5004 (1999).
[19] H. L. Berghout, F. F. Crim, M. Zyrianov, and H. Reisler, J. Chem. Phys. **112**, 6678 (2000).
[20] H. L. Berghout, S. Hsieh, and F. F. Crim, J. Chem. Phys. **114**, 10835 (2001).
[21] H. Xu, Y. Guo, S. Liu, X. Ma, D. Dai, and G. Sha, J. Chem. Phys. **117**, 5722 (2002).
[22] J. Liu, F. Y. Wang, H. Wang, B. Jiang, and X. M. Yang, J. Chem. Phys. **122**, 104309 (2005).
[23] J. Liu, F. Y. Wang, H. Wang, B. Jiang, and X. M. Yang, Chin. J. Chem. Phys. **19**, 1 (2006).
[24] J. J. Lin, J. Zhou, W. Shiu, and K. Liu, Rev. Sci. Instrum. **74**, 2495 (2003).
[25] D. H. Parker and A. T. J. B. Eppink, J. Chem. Phys. **107**, 2357 (1997).
[26] W. S. Drozdoski, A. P. Baronavski, and J. R. McDonald, Chem. Phys. Lett. **64**, 421 (1979).
[27] R. N. Zare, Mol. Photochem. **4**, 1 (1972).
[28] R. G. Bray and R. M. Hochstrasser, Mol. Phys. **31**, 1199 (1976).
[29] D. W. Neyer, A. J. R. Heck, and D. W. Chandler, J. Chem. Phys. **110**, 3411 (1999).
[30] A. V. Demyanenko, V. Dribinski, H. Reisler, H. Meyer, and C. X. W. Qian, J. Chem. Phys. **111**, 7383 (1999).

DOI:10.1088/1674-0068/20/04/388-394